

NANO EXPRESS

Open Access



Tuning of Thermoelectric Properties of MoSe₂ Thin Films Under Helium Ion Irradiation

Hyuk Jin Kim¹, Nguyen Van Quang², Thi Huong Nguyen², Sera Kim³, Yangjin Lee⁴, In Hak Lee⁵, Sunglae Cho², Maeng-Je Seong³, Kwanpyo Kim⁴ and Young Jun Chang^{1,6*} 

Abstract

Transition metal dichalcogenides have attracted renewed interest for use as thermoelectric materials owing to their tunable bandgap, moderate Seebeck coefficient, and low thermal conductivity. However, their thermoelectric parameters such as Seebeck coefficient, electrical conductivity, and thermal conductivity are interdependent, which is a drawback. Therefore, it is necessary to find a way to adjust one of these parameters without affecting the other parameters. In this study, we investigated the effect of helium ion irradiation on MoSe₂ thin films with the objective of controlling the Seebeck coefficient and electrical conductivity. At the optimal irradiation dose of 10¹⁵ cm⁻², we observed multiple enhancements of the power factor resulting from an increase in the electrical conductivity, with slight suppression of the Seebeck coefficient. Raman spectroscopy, X-ray diffraction, and transmission electron microscopy analyses revealed that irradiation-induced selenium vacancies played an important role in changing the thermoelectric properties of MoSe₂ thin films. These results suggest that helium ion irradiation is a promising method to significantly improve the thermoelectric properties of two-dimensional transition metal dichalcogenides.

Keywords: MoSe₂, Helium ion irradiation, Thermoelectric property, Seebeck coefficient

Introduction

Transition metal dichalcogenides (TMDCs) have attracted considerable attention as two-dimensional (2D) material candidates beyond graphene owing to their unique electronic, optical, mechanical, chemical, and thermal properties [1]. They comprise one transition metal atom (i.e., Mo or W) and two chalcogen atoms (i.e., S, Se, or Te). The hexagonal metal layer is sandwiched by two hexagonal chalcogen layers, while the interface between the chalcogen layers is weakly bonded through van der Waals bonding. Such weak van der Waals bonding allows exfoliation of individual layers, stacking of arbitrary heterostructures, intercalation of charged ions

(Li⁺ or Na⁺), and low thermal conductivity in the vertical direction [2–4]. In particular, semiconducting compounds, such as MX₂ (M = Mo, W, or Re; X = S or Se), have been intensively investigated for their novel electronic and optical properties such as direct–indirect band gap transition [1, 5], large exciton signal [6], valley polarization [7], anisotropic electronic properties [8], and thermoelectric properties [9, 10].

Thermoelectric properties of TMDCs, especially, have been investigated because of diverse electronic properties, low thermal conductivity, and moderate Seebeck coefficient [11]. The energy conversion efficiency of thermoelectric materials is related to a dimensionless figure of merit ZT given by $ZT = \frac{\alpha^2 \sigma}{\kappa} T$, where α is the Seebeck coefficient, σ is the electrical conductivity, κ is the thermal conductivity, T is the average temperature, and $\alpha^2 \sigma$ is the thermoelectric power factor. For the improvement of the thermoelectric performance, or achievement

*Correspondence: yjchang@uos.ac.kr

¹ Department of Physics, University of Seoul, 163 Siripdaero, Dongdaemun-gu, Bldg 14-217, Seoul 02504, Republic of Korea
Full list of author information is available at the end of the article

of a high ZT value, α and σ should be increased and κ should be decreased. However, these three parameters are adversely interdependent, and therefore, tuning one parameter inevitably changes the other parameters. Attempts have been made to overcome this problem, for instance, through the fabrication of nanostructures or ion-beam-induced defect engineering. Nanostructures, such as nanowires, nanosheets, nanohole patterns, or superlattices, have considerably low thermal conductivity owing to increased phonon scattering [12].

Irradiation of TMDCs with ion beams, such as hydrogen or helium ions (He^+), induces defects, such as dislocations, interstitials, and vacancies, and thereby strongly influences the crystalline order, electrical, and thermoelectric properties [13–15]. He^+ has a low mass, a small atomic radius, and a low scattering cross section in comparison with heavy atoms, such as Ne^+ , Ar^+ , and Kr^+ . The heavier atoms often ablate the sample surface and form amorphous phase, so that they are employed for surface removal or sputtering. On the other hand, He^+ can be employed for wide range applications, such as gentle modification of whole thin film devices [15], helium ion microscopy [16], and focused ion milling [17], depending on the acceleration energy and dose. The Seebeck coefficient is obtained from the Mott relation $\alpha \propto m^*/n$, where m^* is the effective mass and n is the carrier concentration [11], and the electrical conductivity can be written as $\sigma = en\mu$, where e is the carrier charge and μ is the electrical mobility. Ion irradiation increases the carrier concentration but also induces structural defects, which then decreases the carrier mobility and the lattice thermal conductivity. Such intertwined influences of ion irradiation on the carrier transport properties may result in nonlinear behaviors of thermoelectric properties for the ion irradiation. In addition, the suppressed lattice thermal conductivity may enhance the ZT value.

Recent theoretical calculations have yielded a high ZT ($=1$) for semiconducting TMDCs, that is, $\text{Mo}(\text{S}, \text{Se})_2$ and WSe_2 [18–20]. Based on the first-principles calculations or molecular dynamics method, the intrinsic electrical and thermal properties of pristine TMDCs are theoretically studied and their differences with the experiments are maybe due to the pristine nature of their simulation models. Notably, a high Seebeck coefficient ($\alpha = 10$ mV/K) [9] and large variations of thermal conductivities (0.05–40 W/(m K)) [4, 21, 22] have been experimentally observed. Furthermore, the mechanical flexibility of TMDCs and their atomically thin layers render them promising materials for use in wearable electronics; it has been shown that a prototype thermoelectric wearable device with a combination of chemically exfoliated n -type WS_2 and p -type NbSe_2 generates an electrical power when a temperature gradient exists

on the human body [23]. However, in-depth studies on the optimization of thermoelectric properties of TMDCs thin films via ion irradiation are scarce.

In this study, we investigated the use of He^+ irradiation for improving the thermoelectric properties of MoSe_2 thin films. Raman spectroscopy and high-resolution X-ray diffraction (HRXRD) measurements were made to analyze changes in the phonon vibration mode and crystal structure of the thin films, respectively, and transmission electron microscopy (TEM) and energy-dispersive X-ray spectroscopy (EDS) were used to detect microscopic atomic disorders and determine chemical stoichiometries, respectively. Furthermore, the dependence of the Seebeck coefficient and electrical conductivity on the irradiation dose was examined.

Methods

MoSe_2 thin films were grown on a mica muscovite substrate in a high-vacuum co-evaporation chamber with a base pressure below 5×10^{-8} Torr. High-purity Mo (99.95%) and Se (99.999%) were simultaneously evaporated from an electron-beam evaporator and a Knudsen cell at rates of 0.1 and 1.5 Å/s, respectively, with the substrate temperature being maintained at 260°C [24, 25]. The film thicknesses were determined through calibration with a quartz crystal oscillator and verified by cross-sectional TEM analysis, and they were about 30 nm. Thin film growth was followed by cooling, without post-annealing. The thin films were irradiated with a 30 keV He^+ beam obtained from an ion accelerator installed at the Korea Multi-purpose Accelerator Complex (KOMAC, Gyeongju, Korea). The selected He^+ doses were 10^{14} , 10^{15} , and 10^{16} cm $^{-2}$, and they are hereafter referred to as He-14, He-15, and He-16, respectively. After the He^+ irradiation, the samples were taken from the facility after a few days because the radioactive level of the samples should be below the certain safety level. The previous real-time monitoring of electrical properties of graphene during irradiation shows fast saturating behavior just after the irradiation event [26, 27]. Therefore, we may expect the most physical properties of irradiated samples are saturated to certain values when we analyze afterward.

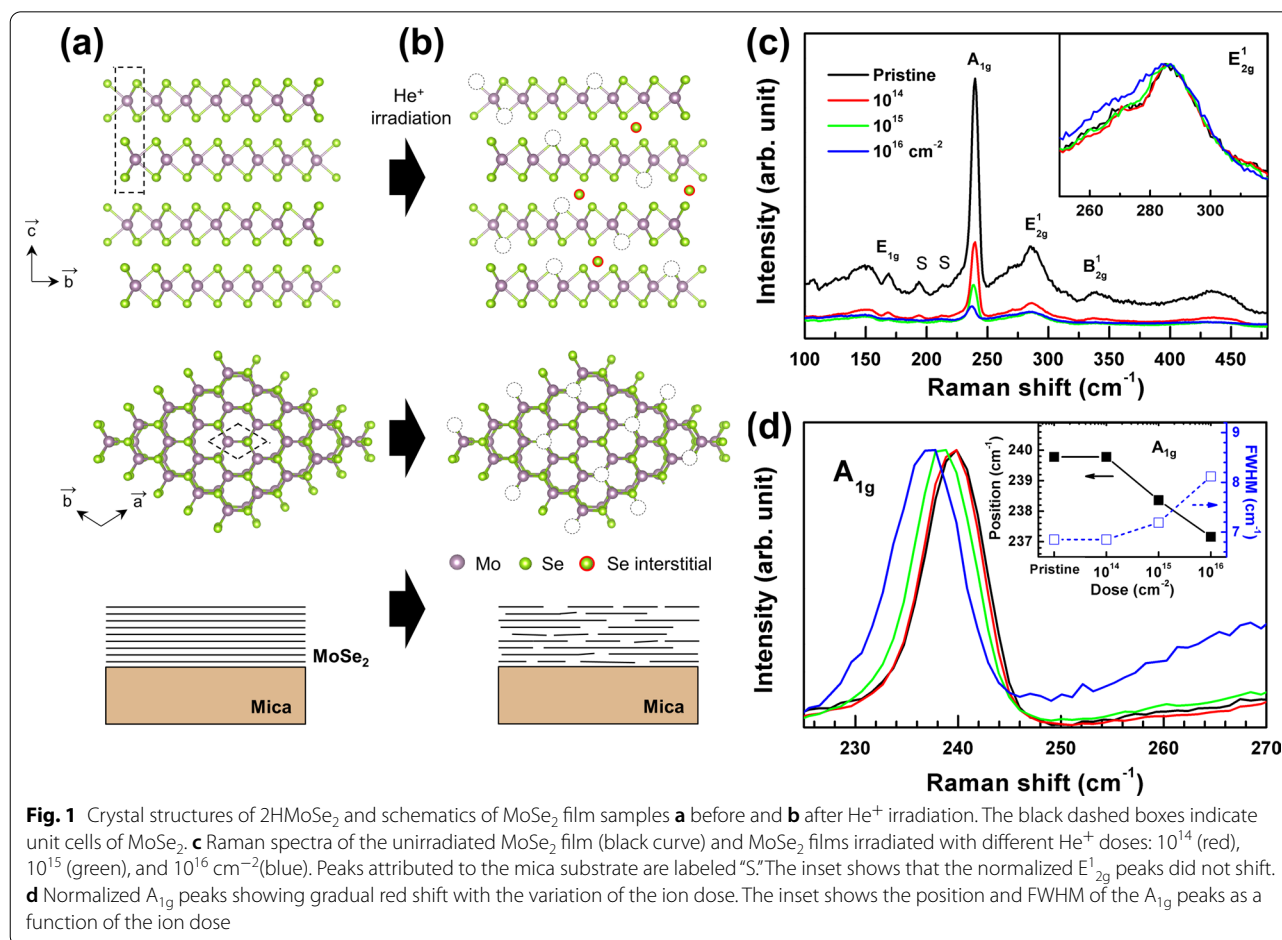
Raman spectroscopy measurements were taken using a 532-nm excitation laser source with a fixed power (30 mW) and a fixed acquisition time (60 s) at room temperature. Scattered light from the samples was analyzed using a single-grating monochromator with a focal length of 50 cm, and it was detected by a liquid-nitrogen-cooled charge-coupled-device detector [28]. HRXRD measurements were made using an in-house X-ray diffractometer (D8, Bruker) with $\text{Cu K}\alpha_1$ radiation, and the film microstructure was studied using TEM (JEM-2100F

and JEM-ARM200F, JEOL) at an accelerating voltage of 200 kV. Cross-sectional film samples for TEM were fabricated by focused-ion-beam (Helios Nanolab 450, FEI), and plan-view TEM samples of MoSe₂ film were prepared by the wet transfer method. Chemical stoichiometries were analyzed using EDS from field-emission scanning electron microscopy (FE-SEM, SU8101, Hitachi) measurements. The Seebeck coefficient and electrical conductivity were simultaneously measured from 300 to 420 K by using a home-built thermoelectric measurement system, which is described elsewhere [29].

Results and Discussion

Figure 1a shows an atomic model of 2H phase MoSe₂; top and side views of the compound are shown, and the dashed boxes indicate unit cells. MoSe₂ has a trigonal prismatic crystal structure, D_{3h} point group symmetry, and a 2D layered structure with van der Waals bonding [30]. We chose mica substrates for fabricating flat films and minimized wrinkle formation during their growth [24]. Mica substrates have been widely used for van der Waals epitaxial growth of TMDC thin

films owing to their atomically flat surface and absence of dangling bonds [31]. Figure 1c shows Raman spectra of He⁺-irradiated MoSe₂ thin films. The pristine sample shows A_{1g}, E_{1g}, E_{2g}¹, and B_{2g}¹ modes, which correspond to out-of-plane (A_{1g} and B_{2g}¹) and in-plane (E_{1g} and E_{2g}¹) phonon vibrations. The peak positions are consistent with those of MoSe₂ bulk and thick films [5]. The mica substrate contributed three small peaks, labeled by the letter “S.” Raman peak intensities are inversely proportional to defect formation and disorder for a crystalline lattice. As the He⁺ dose increased, the Raman peak intensities reduced in the entire measurement range, indicating that the He⁺ beam introduced significant defects or disorder in both the films and substrates. Notably, the A_{1g} peak shifted from 239.8 cm⁻¹ (pristine) to 237.2 cm⁻¹ (He-16) and its full width at half-maximum (FWHM) also increased from 6.9 to 8.1 cm⁻¹ (Fig. 1d) as the He⁺ dose increased. By contrast, the inset of Fig. 1c shows that the E_{2g}¹ peak did not shift. Raman peak positions of TMDCs are sensitive to the layer thickness [5], presence of the thermal effect [32], number of point defects (i.e., vacancies) [33], and strain state [34], and among these,

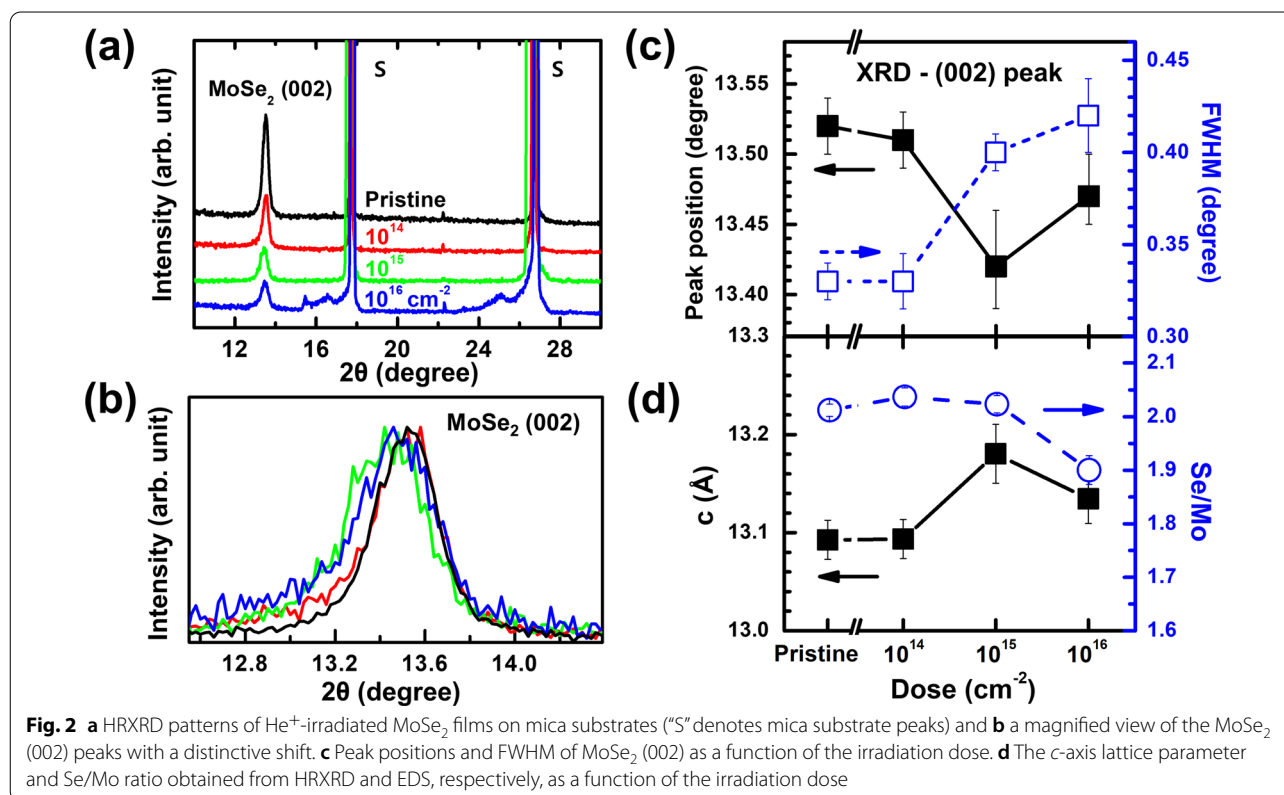


a change in the number of point defects or strain state would be the most probable cause for the change in the A_{1g} peak. Furthermore, notably, only the out-of-plane vibration A_{1g} mode is sensitively shifted, which rules out the possibility of any changes in the strain state. Thus, Raman analysis indicated the generation of a significant amount of defects and disorder in the MoSe_2 thin films by He^+ irradiation, which is consistent with the case of He^+ -irradiated MoS_2 [13].

To compare the crystalline state for different irradiation doses, we performed HRXRD measurements, shown in Fig. 2a, for the series of MoSe_2 thin films. The pristine MoSe_2 film showed a characteristic (002) peak at 13.5° , which matched that of the 2H MoSe_2 phase. The c -axis lattice constant was determined to be 13.09 Å, which was close to those of bulk and thin films [25, 30]. Absence of peaks other than the strong (002) peak indicated well-stacked layered growth along the c -axis of the mica substrates. The strong peaks at $2\theta = 17.5^\circ$ and 26.5° corresponded to the (001) and (002) planes of the mica substrate, respectively [35]. When the films were irradiated with the He^+ beam, the (002) peak's intensity gradually decreased and shifted toward lower angles. As evident in Fig. 2b, the normalized MoSe_2 (002) peak shifted and its FWHM increased. We compared the peak positions and FWHM as a function

of the irradiation dose, as shown in Fig. 2c. Interestingly, both peak position and FWHM values started to change significantly when the He^+ dose exceeded 10^{15} cm^{-2} . Consequently, the extracted c -axis lattice parameter increased by 0.4% (Fig. 2d), consistent with the shift in the A_{1g} peak (out-of-plane mode).

To examine stoichiometric variation, we performed EDS analysis from FE-SEM measurements without sample transfer. Atomic percentage ratios of Se/Mo were extracted from the EDS spectrum for all the samples, and they are shown in Fig. 2d. The Se/Mo ratio ranged from 2.01 (pristine sample) to 1.90 (He-16 sample). We speculate that the initial He^+ irradiation (He-14) introduced crystalline disorder without affecting the Se/Mo ratio, possibly generating atomic vacancies and interstitials. A much higher irradiation dose (He-16) reduced the Se content and significantly disturbed the in-plane crystalline order, as shown schematically in Fig. 1b. First-principles studies have shown that the formation of chalcogen vacancies is energetically preferred over transition metal vacancies [36]. The mass of Se is 1.2 times smaller than that of Mo, and consequently He^+ ions transfer more energy to Se atoms than to Mo atoms during collisions. Notably, preferential sputtering of light atoms in MoS_2 has been observed for irradiation with He^+ and electron beams [13].



To understand the microscopic effects of He^+ irradiation of layered MoSe_2 , we performed a series of TEM analyses, and TEM images of the pristine sample and He-15 sample are shown in Fig. 3. Cross-sectional TEM was used to study the layered structure, and plan-view TEM was used to investigate the lattice arrangement of atoms. In Fig. 3a, the low-magnification bright-field cross-sectional TEM image shows uniform film growth with a thickness of 30 nm. The pristine sample shows a well-stacked layered structure with uniform contrast and thickness on the surface plane of the mica substrate. This indicates that atomically flat mica substrates are ideal for fabricating layered MoSe_2 thin films [31]. On the other hand, the He-15 sample shows a more disordered stacking with largely wiggling patterns, indicating the presence of grain boundaries and dislocations, as expected from the Raman and HRXRD analyses (Fig. 3b). Figure 3c, d shows plan-view TEM images with their fast Fourier transformation (FFT) images. The pristine sample showed a well-ordered hexagonal lattice, and the lattice

constant ($a = 3.3 \text{ \AA}$) determined from the plan-view TEM images corresponded to that of bulk 2H MoSe_2 [30]. Plan-view TEM images also show local structural disorders, such as grain boundaries, defects, and dislocations. Although some of defects may have originated during the transfer of the fabricated film onto the TEM grid, we examine the possibility of film damage after He^+ irradiation. The FFT image of the pristine sample showed quite sharp diffraction peaks (inset of Fig. 3c). In the He-15 sample, the degree of disorder significantly increased, while the corresponding FFT showed broadened patterns. TEM analysis provided microscopic evidence of crystalline disorders or defects for He^+ dose beyond a threshold value. When increasing the He^+ dose, both the Raman and XRD peaks are drastically suppressed, and the TEM images demonstrate local atomic structural disorders. Therefore, through the comprehensive analyses, such as Raman, XRD, and TEM, we demonstrate that crystalline disorder increases as the He^+ dose increases.

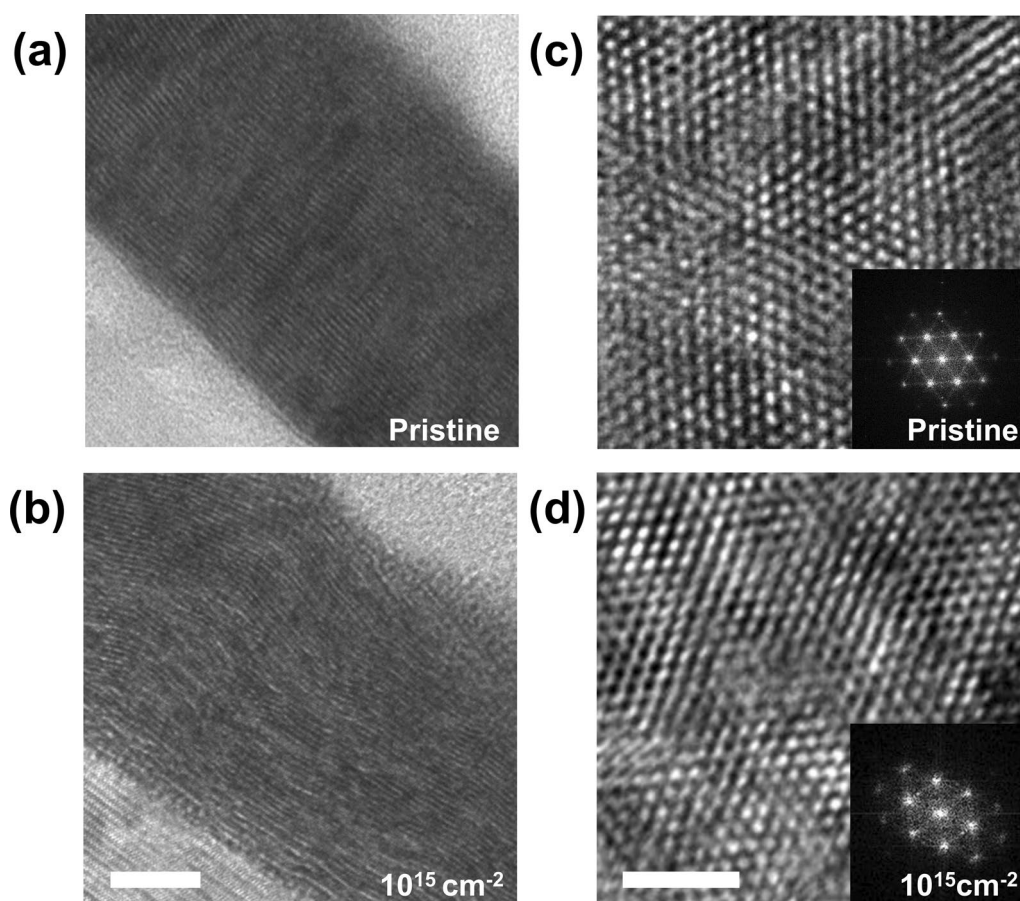


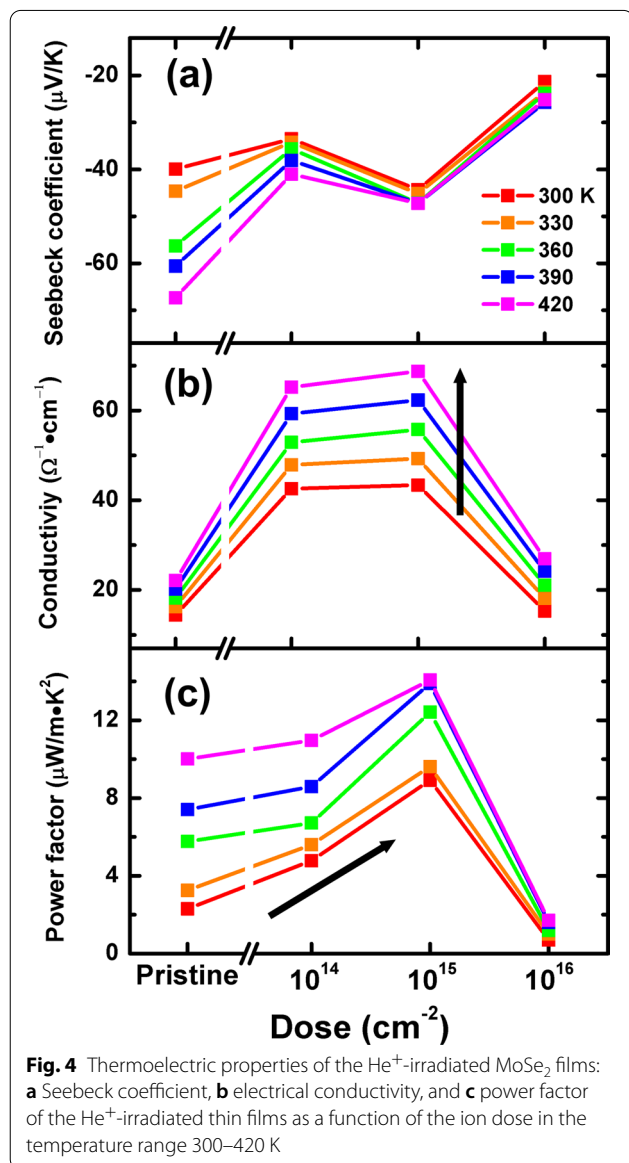
Fig. 3 Cross-sectional TEM images of **a** the pristine sample and **b** the He-15 sample (scale bar = 10 nm). Plan-view TEM images of **c** the pristine sample and **d** the He-15 sample (scale bar = 2 nm). The insets show the corresponding FFT images

We next performed the thermoelectric characterization of the films. The uniformly continuous nature of the films and the insulating mica substrate enabled us to perform temperature-dependent Seebeck and electrical conductivity measurements of the as-grown films from 300 to 420 K. In Fig. 4a, all samples show negative Seebeck coefficients, indicating that electrons were the dominant carriers. The pristine sample shows strong temperature dependence of the Seebeck coefficient. The temperature dependence is considerably reduced with an increase in the irradiation dose, while the magnitude of the Seebeck coefficient gradually decreases. Figure 4b shows the electrical conductivity as a function of the temperature and dose. All the samples show similar

insulating behavior, with the conductivity increasing with the temperature (the arrow in Fig. 4b). With an increase in the ion dose, the conductivity sharply increased up to 10^{15} cm^{-2} and then dropped at 10^{16} cm^{-2} . The thermoelectric power factor showed nonlinear dependence on the dose (Fig. 4c), and it showed a gradual increase when the dose was increased up to 10^{15} cm^{-2} . However, the sharp decrease in both Seebeck coefficient and conductivity minimized the thermoelectric power factor. Notably, the maximum power factor value of $13 \mu\text{W}/\text{m K}^2$ was obtained at 420 K for the He-15 sample.

We explain the observed thermoelectric properties based on our microscopic understanding of the MoSe_2 films under He^+ irradiation. From the analysis discussed above, we note that He^+ irradiation initially induced crystalline defects and then degraded the lattice structure, apart from introducing a significant number of Se vacancies. A small number of defects, such as vacancies or interstitials, are likely to increase the carrier concentration. An increase in the number of carriers enhances the conductivity but decreases the Seebeck coefficient, in accordance with the Mott relation, as discussed in Introduction section. However, a higher dose of ion irradiation (He-16) significantly damaged the crystalline phase by introducing Se vacancies. The resulting high level of structural disorder caused significant scattering of charge carriers and degraded the carrier mobility, which explains degradation of the conductivity. In other words, the dose increases the carrier concentration but also introduces structural disorders, which then diminishes the carrier transport characteristics explain the nonlinear tendency of thermoelectric properties with respect to the He^+ dose. It is also noted that the structural disorder also induced scattering of phonon transport and suppress the lattice thermal conductivity, which then may increase the ZT value of the materials [11].

Finally, our result demonstrates that the use of ion irradiation is a very powerful approach to enhance the thermoelectric performance of 2D materials. The maximum power factor value of $13 \mu\text{W}/\text{m}\cdot\text{K}^2$ was obtained at 420 K, which is comparable to other TMDC nanosheets, single-walled nanotubes, and some organic materials [23, 37, 38]. We also observed that optimum irradiation (10^{15} cm^{-2}) could increase the power factor value of the MoSe_2 films by ~ 4 times at 300 K. In view of the reported power factor values of TMDC materials ($5\text{--}80 \mu\text{W}/\text{m K}^2$) [9–11], it would be of considerable interest to use the ion irradiation method to improve their thermoelectric properties. Also, the similar approach of He^+ irradiation to improve thermoelectric performance can be extended to improve thermoelectric device performance by inserting a He^+ irradiation step into device fabrication process. In



a previous report, flexible thermoelectric device applications utilized similar TMDC compounds, such as WS_2 - $NbSe_2$, in which power factor of WS_2 component reaches $6 \mu W/m \cdot K^2$ [23]. Furthermore, this approach is well matched in typical thermoelectric materials such as Bi_2Te_3 and Sb_2Te_3 . Although Bi_2Te_3 is differentiated from TMDC in that Bi_2Te_3 has rhombohedral crystal structure and 3D topological insulating electronic structure, ion irradiation improves thermoelectric characteristics by a factor of two in Bi_2Te_3 nanorod and organic/ Bi_2Te_3 composite film [39]. Therefore, the effectiveness of the ion irradiation technique suggests that it can be used for universal tuning of the thermoelectric properties of various materials, including TMDCs and other 2D layered materials.

Conclusion

To summarize, we investigated the use of He^+ irradiation for controlling the thermoelectric properties of $MoSe_2$ thin film by varying the irradiation dose. The use of an irradiation dose beyond a threshold value caused crystal-line defects and chemical disorder, which were evidenced by Raman, HRXRD, and TEM analyses. We found that irradiation-induced defects increased the electrical conductivity while slightly reducing the Seebeck coefficient. The irradiation dose was varied up to 10^{16} cm^{-2} , and the maximum value of the power factor of the $MoSe_2$ thin films was obtained at 10^{15} cm^{-2} . Along with the low thermal conductivity values of TMDCs, the observed increase in the power factor with the irradiation dose indicated high thermoelectric performances of the TMDCs. Furthermore, our result shows that the use of helium ion irradiation and irradiation-based approaches has high potential for use in the development of high-performance thermoelectric devices.

Abbreviations

TMDC: Transition metal dichalcogenide; He^+ : Helium ion; HRXRD: High-resolution X-ray diffraction; TEM: Transmission electron microscopy; EDS: Energy-dispersive X-ray spectroscopy; FE-SEM: Field-emission scanning electron microscopy; FWHM: Full-width half maximum; FFT: Fast Fourier transformation.

Acknowledgements

There is no acknowledgement.

Authors' Contributions

HJK helped in synthesis, characterization, and original draft preparation; NVQ, THN, SC performed thermoelectric investigation; SK, MJS helped in Raman investigation; YL, KK were involved in TEM investigation; IHL contributed to characterization and analysis; YJC helped in supervision and reviewing. All authors read and approved the final manuscript.

Funding

This work was supported by the National Research Foundation (NRF) grants funded by the Korean government (Nos. NRF-2020R1A2C200373211, 2020R1A5A1016518, 2020K1A4A7A02095438). Part of this study has been performed using facilities at IBS Center for Correlated Electron Systems, Seoul National University. This research was supported by Nano-Material Technology

Development Program through the National Research Foundation of Korea (NRF) funded by the Ministry of Science, ICT and Future Planning, Korea (2009-0082580).

Availability of Data and Materials

The datasets supporting the conclusions of this article are included within the article.

Declarations

Competing Interests

The authors declare that they have no competing interests.

Author details

¹Department of Physics, University of Seoul, 163 Siripdaero, Dongdaemun-gu, Bldg 14-217, Seoul 02504, Republic of Korea. ²Department of Physics and Energy Harvest Storage Research Center, University of Ulsan, Ulsan 44610, Republic of Korea. ³Department of Physics, Chung-Ang University, Seoul 06974, Republic of Korea. ⁴Department of Physics, Yonsei University, Seoul 03722, Republic of Korea. ⁵Center for Spintronics, Korea Institute of Science and Technology, Seoul 02792, Republic of Korea. ⁶Department of Smart Cities, University of Seoul, Seoul 02504, Republic of Korea.

Received: 18 October 2021 Accepted: 30 January 2022

Published online: 10 February 2022

References

- Wang QH, Kalantar-Zadeh K, Kis A et al (2012) Electronics and optoelectronics of two-dimensional transition metal dichalcogenides. *Nat Nanotechnol* 7:699
- Yang E, Ji H, Jung Y (2015) Two-dimensional transition metal dichalcogenide monolayers as promising sodium ion battery anodes. *J Phys Chem C* 119:26374–26380
- Geim AK, Grigorieva IV (2013) Van der Waals heterostructures. *Nature* 499:419
- Chiritescu C, Cahill DG, Nguyen N, et al (2007) Ultralow thermal conductivity in disordered, layered WSe_2 crystals. *Science* (80-) 315:351 LP-353
- Tonndorf P, Schmidt R, Böttger P et al (2013) Photoluminescence emission and Raman response of monolayer MoS_2 , $MoSe_2$, and WSe_2 . *Opt Express* 21:4908–4916
- Mueller T, Malic E (2018) Exciton physics and device application of two-dimensional transition metal dichalcogenide semiconductors. *npj 2D Mater Appl* 2:29
- Schaibley JR, Yu H, Clark G et al (2016) Valleytronics in 2D materials. *Nat Rev Mater* 1:16055
- Choi BK, Ulstrup S, Gunasekera SM et al (2020) Visualizing orbital content of electronic bands in anisotropic 2D semiconducting $ReSe_2$. *ACS Nano* 14:7880–7891
- Wu J, Schmidt H, Amara KK et al (2014) Large thermoelectricity via variable range hopping in chemical vapor deposition grown single-layer MoS_2 . *Nano Lett* 14:2730–2734
- Huang H, Cui Y, Li Q et al (2016) Metallic 1T phase MoS_2 nanosheets for high-performance thermoelectric energy harvesting. *Nano Energy* 26:172–179
- Zhang G, Zhang Y-W (2017) Thermoelectric properties of two-dimensional transition metal dichalcogenides. *J Mater Chem C* 5:7684–7698
- Mao J, Liu Z, Ren Z (2016) Size effect in thermoelectric materials. *npj Quantum Mater* 1:16028
- Fox DS, Zhou Y, Maguire P et al (2015) Nanopatterning and electrical tuning of MoS_2 layers with a subnanometer helium ion beam. *Nano Lett* 15:5307–5313
- Stanford MG, Pudasaini PR, Belianinov A et al (2016) Focused helium-ion beam irradiation effects on electrical transport properties of few-layer WSe_2 : Enabling nanoscale direct write homo-junctions. *Sci Rep* 6:1–10
- Iberi V, Liang L, Ilev AV et al (2016) Nanoforging single layer $MoSe_2$ through defect engineering with focused helium ion beams. *Sci Rep* 6:30481

16. Hlawacek G, Veligura V, van Gastel R, Poelsema B (2014) Helium ion microscopy. *J Vac Sci Technol B* 32:20801
17. Stanford MG, Lewis BB, Mahady K et al (2017) Review article: Advanced nanoscale patterning and material synthesis with gas field helium and neon ion beams. *J Vac Sci Technol B* 35:30802
18. Huang W, Luo X, Gan CK et al (2014) Theoretical study of thermoelectric properties of few-layer MoS_2 and WSe_2 . *Phys Chem Chem Phys* 16:10866–10874
19. Kumar S, Schwingenschlöggl U (2015) Thermoelectric response of bulk and monolayer MoSe_2 and WSe_2 . *Chem Mater* 27:1278–1284
20. Kandemir A, Yapiçioğlu H, Kinacı A et al (2016) Thermal transport properties of MoS_2 and MoSe_2 monolayers. *Nanotechnology* 27:55703
21. Hadland EC, Jang H, Wolff N, et al (2019) Ultralow thermal conductivity of turbostratically disordered MoSe_2 ultra-thin films and implications for heterostructures. *Nanotechnology* 30:285401
22. Yarali M, Brahmı H, Yan Z et al (2018) Effect of metal doping and vacancies on the thermal conductivity of monolayer molybdenum diselenide. *ACS Appl Mater Interfaces* 10:4921–4928
23. Oh JY, Lee JH, Han SW et al (2016) Chemically exfoliated transition metal dichalcogenide nanosheet-based wearable thermoelectric generators. *Energy Environ Sci* 9:1696–1705
24. Yang SJ, Lee Y, Kim JH et al (2019) Single-step synthesis of wrinkled MoSe_2 thin films. *Curr Appl Phys* 19:273–278
25. Choi BK, Kim M, Jung K-H et al (2017) Temperature dependence of band gap in MoSe_2 grown by molecular beam epitaxy. *Nanoscale Res Lett* 12:492
26. Lee IH, Lee C, Choi BK et al (2018) Proton-induced conductivity enhancement in AlGaIn/GaN HEMT Devices. *J Korean Phys Soc* 72:920–924
27. Lee C, Kim J, Kim S et al (2016) Strong hole-doping and robust resistance-decrease in proton-irradiated graphene. *Sci Rep* 6:21311
28. Kim J, Park W, Lee J-H, Seong M-J (2019) Simultaneous growth of Ga_2S_3 and GaS thin films using physical vapor deposition with GaS powder as a single precursor. *Nanotechnology* 30:384001
29. Duong AT, Rhim SH, Shin Y et al (2015) Magneto-transport and thermoelectric properties of epitaxial FeSb_2 thin film on MgO substrate. *Appl Phys Lett* 106:32106
30. Hu SY, Liang CH, Tiong KK et al (2005) Preparation and characterization of large niobium-doped MoSe_2 single crystals. *J Cryst Growth* 285:408–414
31. Vergnaud C, Dau M-T, Grévin B, et al (2020) New approach for the molecular beam epitaxy growth of scalable WSe_2 monolayers. *Nanotechnology* 31:255602
32. Thripuranthaka M, Kashid RV, Sekhar Rout C, Late DJ (2014) Temperature dependent Raman spectroscopy of chemically derived few layer MoS_2 and WS_2 nanosheets. *Appl Phys Lett* 104:81911
33. Mahjouri-Samani M, Liang L, Oyedele A et al (2016) Tailoring vacancies far beyond intrinsic levels changes the carrier type and optical response in monolayer MoSe_{2-x} crystals. *Nano Lett* 16:5213–5220
34. Cheng X, Jiang L, Li Y, et al (2020) Using strain to alter the energy bands of the monolayer MoSe_2 : A systematic study covering both tensile and compressive states. *Appl Surf Sci* 521:146398
35. Zheng M, Sun H, Kwok KW (2019) Mechanically controlled reversible photoluminescence response in all-inorganic flexible transparent ferroelectric/mica heterostructures. *NPG Asia Mater* 11:52
36. Komsa H-P, Krasheninnikov AV (2015) Native defects in bulk and monolayer MoS_2 from first principles. *Phys Rev B* 91:125304
37. Nonoguchi Y, Ohashi K, Kanazawa R et al (2013) Systematic conversion of single walled carbon nanotubes into n-type thermoelectric materials by molecular dopants. *Sci Rep* 3:3344
38. Russ B, Glauđell A, Urban JJ et al (2016) Organic thermoelectric materials for energy harvesting and temperature control. *Nat Rev Mater* 1:16050
39. Sinduja M, Amirthapandian S, Magudapathy P, Srivastava SK, Asokan K (2018) Tuning of the thermoelectric properties of Bi_2Te_3 nanorods using helium ion irradiation. *ACS Omega* 3:18411–18419

Publisher's Note

Springer Nature remains neutral with regard to jurisdictional claims in published maps and institutional affiliations.

Submit your manuscript to a SpringerOpen® journal and benefit from:

- Convenient online submission
- Rigorous peer review
- Open access: articles freely available online
- High visibility within the field
- Retaining the copyright to your article

Submit your next manuscript at ► [springeropen.com](https://www.springeropen.com)